

ERS-1 Scatterometer Estimates of Annual Variations of Atlantic ITCZ and Pacific NECC

D. Halpern<sup>1</sup>, M. H. Freilich<sup>2</sup> and R. S. Dunbar<sup>3</sup>

<sup>1</sup> Earth and Space Sciences Division

**Jet Propulsion Laboratory**

California Institute of Technology

Pasadena, CA 91109

<sup>2</sup> School of oceanography

Oregon State University

Corvallis, OR 97331

<sup>3</sup> Telecommunications Science and Engineering Division

**Jet Propulsion Laboratory**

California Institute of Technology

Pasadena, CA 91109

## ABSTRACT

Freilich and Dunbar (1993) produced a 10-m height wind vector data set, named CMODIFD, from the European Space Agency (ESA) first European Remote Sensing (ERS-1) Active Microwave instrument (AMI) measurement. The CMODIFD wind vectors compared favorably with moored-buoy wind observations at about 60 sites. Satisfactory results were obtained from intercomparisons between CMODIFD and moored-buoy estimates of horizontal wind divergence and wind-stress curl. The CMODIFD positions of the Intertropical Convergence Zone (ITCZ) at 28°W were nearly equal to those determined from Satellite images of clouds. The CMODIFD data were employed to compute the Ekman vertical velocity in the region of the Pacific North Equatorial Countercurrent (NECC), and a correlative relation was found between the annual cycles and longitudinal variations of the NECC and Ekman vertical motion.

### 1. INTRODUCTION

Further understanding of the monthly mean dynamics of the North Equatorial Countercurrent (NECC) and the Intertropical Convergence Zone (ITCZ) requires knowledge of relatively small-scale horizontal gradients of the surface wind field. Because the latitudinal widths of the NECC and ITCZ are approximately 500 and 200 km, respectively, the usual sources of surface wind information are not adequate. Horizontal dimensions of surface wind data products from numerical weather prediction forecast-analysis systems are too large (typically 200 km x 200 km) to describe ocean-atmosphere interactions associated with the NECC and ITCZ. Observations of surface winds from ships are too sparse. Only satellites provide frequent coverage of surface winds. The European Space Agency (ESA) first European Remote Sensing (ERS-1) wind scatterometer measurements are used to determine surface wind convergence in the Atlantic ITCZ and the Ekman vertical velocity in the Pacific NECC.

## 2. EVALUATION OF SCATTEROMETER WINDS

The 5.3-GHz (C-band) Active Microwave Instrument (AMI) was mounted on ERS-1, which was launched 17 July 1991. The AMI is an active microwave radar which measures the strength of resonant Bragg scattering produced from approximately 5-cm wavelength surface waves created by the wind. The 3-antennae scatterometer was designed to measure 10-m height wind speed and direction with accuracies of  $2 \text{ m s}^{-1}$  and  $20^\circ$  (ESA, 1992) within 50-km diameter cells with the centers spaced at 25-km intervals in a 500-km swath. The swath center is located 450 km to the right of the direction of the spacecraft.

The model function relating the AMI-measured normalized molar cross section,  $\sigma_0$  (sigma-naught), and 10-m height wind speed and direction for neutral stratification is complex, and no universal relationship exists. The  $\sigma_0$  measurements were continuously determined by ESA after 1 January 1992.; prior to this date, there were long intervals when  $\sigma_0$  was not estimated. Calibration of the AMI was modified in March 1992, and no further changes were made afterwards. During January 1992. - July 1993 (when the most recent data were acquired), ESA used a succession of three model functions (CMOD2, 1 January -9 June 1992; CMOD3, 10 June 1992-23 February 1993; CMOD4, 24 February -31 July 1993), which were developed at the European Center for Medium-Range Weather Forecasts (ECMWF), to compute surface wind vectors from  $\sigma_0$ . Other groups, such as Centre National de Recherches Météorologiques (METEO-France) and the Institut Français de Recherche et d'Exploitation de la Mer (IFREMER), have developed model functions for various segments of the ERS-1 data set. Freilich and Unhar (1993) developed a model function, CMODFD, which is based upon  $\sigma_0$  measurements collocated with National Meteorological Center (NMC) surface wind analysis. This model function is used to compute 10-m height wind vectors between  $60^\circ\text{S} - 60^\circ\text{N}$ , which we call CMODFD data. We use CMODFD data because the January - June 1992 CMODFD data were more accurate than CMOD2 data (Halpern *et al.*, 1993) and the CMODFD data are the only known ERS-1 wind vector data of at least 18-month duration that is produced with a time-invariant processing method.

What is the proper reference data set to evaluate satellite observations of the surface wind components? No reference data set is free of errors. Wind measurements recorded on ships have a root-mean-square (rms) accuracy of 3 - 4 m s<sup>-1</sup> (Wilkerson and Earle, 1990; Esbensen *et al.*, 1993) and mean bias relative to moored-buoy data of about 1.5 m s<sup>-1</sup> (Wilkerson and Earle, 1990). Operational forecast-analysis of surface winds are not processed uniformly in time because of frequent changes to the forecast-analysis system. Moored-buoy wind measurements at about 4-m height may produce a wind speed lower than the actual speed because of wave sheltering when the wind speed is greater than about 10 m s<sup>-1</sup>. We chose moored-buoy wind data to be the reference data set for comparisons with CMODFD because of a belief that the moored-buoy wind observations are more representative of the wind field than either ship measurement or operational wind analyses created at numerical weather prediction centers. Two buoy wind data sets were used: Tropical Oceans Global Atmosphere (TOGA) Tropical Ocean-Atmosphere (TAO) (Jayes *et al.*, 1991), and National Oceanic and Atmospheric Administration (NOAA) National Data Buoy Center (NDBC) (Meindl and Hamilton, 1992). Data processing procedures for the 1()-m height CMODFD and moored-buoy wind data were described by Halpern *et al.* (1993).

## 2.1 Wind Vector

During January - December 1992 there were 50 and 92. monthly mean CMODFD-NDBC and CMODFD-TAO matchups, respectively. Statistics of the orthogonal regression analysis are listed in Table 1. Correlation coefficients between the monthly mean *u* and *v* matchups were significant, according to the Student's *t* test (Press *et al.*, 1986). The 95% level of statistical significance used throughout the paper is 95%. In all cases, the correlation coefficient indicated that at least 50% of the variances were linearly related. The *u* CMODFD-NDBC correlation coefficient (0.98) was statistically different than the *v* correlation coefficient (0.91), according to the Fisher's *z* test (Press *et al.*, 1986), but only by a very slight margin because the normally distributed *z* value was greater than 1.96 by only 0.7. The *u* and *v* CMODFD-TAO correlation coefficients were not statistically

different, indicating that the correspondence between the matchups was almost isotropic in direction. The rms differences between CMODFD-NDBC  $u$  and  $v$  pairs were 0.98 and 0.80  $\text{m s}^{-1}$ , respectively, which were 63% smaller than that between CMODFD-TAO pairs; the difference was significant, according to the  $F$  test (Press *et al.*, 1986). The larger rms differences and smaller correlation coefficients associated with TAO data compared with NDBC data indicated a lack of wind speed sensitivity of sigma-naught at low wind speed.

## 2.2 Wind Divergence

The horizontal wind divergence,  $\text{HD}$ , was computed from

$$\text{HD} = \partial u / \partial x + \partial v / \partial y = \Delta u / \Delta x + \Delta v / \Delta y, \quad (1)$$

where  $\Delta u$  is the difference of the zonal wind components at two sites separated by a distance  $\Delta x$  along the east-west direction,  $\Delta v$  is the difference of the meridional wind components at two sites separated along the north-south direction by a distance  $\Delta y$ , and the positive  $x$  and  $y$  directions are towards east and north, respectively. Positive and negative values of  $\text{HD}$  are called divergence and convergence, respectively.

Three NDBC sites near  $20^\circ\text{N}, 155^\circ\text{W}$  in the vicinity of the Hawaiian Islands were chosen (Figure 1) because it was the smallest horizontal scale, triangular moored-buoy array. Daily values of  $\Delta u / \Delta x$  and  $\Delta v / \Delta y$  were computed between sites A and B and sites C and B, respectively. During January - December 1992 there were 31 daily CMODFD-NDBC HD matchups. The mean CMODFD convergence ( $2.4 \times 10^{-6} \text{ s}^{-1}$ ) was  $0.3 \times 10^{-6} \text{ s}^{-1}$  or about 10% larger than the NDBC estimate of convergence; the difference was not significant. The correlation coefficient (0.78) between CMODFD-NDBC HD matchups was significant.

## 2.3 Wind-Stress Curl

The vertical component of the surface wind-stress curl, WSC, was computed from

$$WSC = \partial\tau_y/\partial x - \partial\tau_x/\partial y = -\Delta\tau_y/\Delta x - \Delta\tau_x/\Delta y, \quad (2)$$

where  $\tau_x$  and  $\tau_y$  are the east-west and north-south components of wind stress, respectively. The wind-stress components are defined by

$$\tau_x = \rho_a C_D u (u^2 + v^2)^{1/2} \quad (3a)$$

and

$$\tau_y = \rho_a C_D v (u^2 + v^2)^{1/2} \quad (3b)$$

where  $\rho_a$  is the density of air ( $1.225 \text{ kg m}^{-3}$ ) in the constant-stress layer and  $C_D$  is a non-dimensional drag coefficient. We used a wind-speed dependent  $C_D$  (Trenberth *et al.*, 1990). Daily values of  $\Delta\tau_y/\Delta x$  and  $\Delta\tau_x/\Delta y$  were computed between sites A and B and sites C and B (Figure 1), respectively. During January - December 1992 the correlation coefficient (0.85) between 31 daily CMODFD-NDBC WSC matchups was significant. The mean NDBC WSC ( $-3.7 \times 10^{-8} \text{ N m}^{-3}$ ) was  $3.2 \times 10^{-8} \text{ N m}^{-3}$  smaller than that computed from CMODFD data. Although the percentage difference between the two mean values was large, the mean bias was not significant because of the large standard deviations ( $9.3$  and  $14.9 \times 10^{-8} \text{ N m}^{-3}$ ) of the means.

### 3. GLOBAL ANNUAL MEAN WIND VECTORS

All  $1/3^\circ \times 1/3^\circ$  monthly mean  $u$  and  $v$  values during July 1992 to June 1993 were averaged within non-overlapping  $2.5^\circ \times 2.5^\circ$  areas, which was an arbitrarily-chosen grid,

The CMODFD data (Figure 2) portrayed the general surface circulation of the atmosphere. From  $30^\circ$ - $60^\circ$  latitudes in the northern and southern hemispheres, the longitudinal-averaged CMODFD zonal wind direction was eastward. Between  $30^\circ\text{S}$  and  $30^\circ\text{N}$  the CMODFD zonal wind direction was westward, except in the North Indian Ocean where the zonal wind component was near zero. Inspection of Figures 2A and 2C shows that the CMODFD wind-stress curl in the  $20^\circ$ - $40^\circ\text{N}$  band would be primarily related to the north-south gradient of the zonal wind stress compared to the east-west gradient of the meridional wind stress. This geographical pattern of wind components is

a fundamental feature of the surface wind field and is necessary to generate mid-latitude ocean circulation gyres and, consequently, the Gulf Stream and Kuroshio Current, The July 1992- June 1993 mean geographical pattern of the CMOFFD zonal wind components (Figures 2A and 2C) over the mid-latitude ocean gyres was qualitatively similar to the climatological-mean annual wind components that have been computed from wind measurements recorded on ships (Hellerman and Rosenstein, 1983) and from the ECMWF wind product (Trenberth *et al.*, 1990).

Along the Pacific equator the CMOFFD u-wind component had an approximate bell-shape pattern, which was consistent with climatological-mean estimates (Wyrtki and Meyers, 1975). However, the maximum magnitude of the mean July 1992- June 1993 zonal component ( $3-4 \text{ m s}^{-1}$ ) was  $2-3 \text{ m s}^{-1}$  less than that anticipated from climatology, perhaps because of the 1991-1993 El Niño episode. East of about  $110^\circ\text{W}$  and west of the date line the wind had nearly equal components (Figure 2A and 2C); this pattern and the predominant westward direction of the trade wind from  $180^\circ$  to  $110^\circ\text{W}$  were consistent with climatology.

The most prominent feature of the CMOFFD v component was the convergence in the  $10^\circ\text{S} - 10^\circ\text{N}$  band in the Atlantic and Pacific Oceans. The strength of the tropical convergence is primarily determined by  $\partial v/\partial y$ , because in the tropics  $\partial v/\partial y$  is much greater than  $\partial u/\partial x$  (Figure 2A and 2C). In the Pacific the convergence north of the equator in the eastern half of the basin is the ITCZ, which is the name also given to the convergence zone in the Atlantic. In the Atlantic Ocean the  $5^\circ\text{S} - 10^\circ\text{N}$  longitudinal-average  $\partial v/\partial y$  was approximately  $4.2 \times 10^{-6} \text{ s}^{-1}$  (Figure 2D). This was 130% greater than the  $10^\circ\text{S} - 10^\circ\text{N}$  longitudinal-average convergence in the Pacific Ocean (Figure 2D). In the Atlantic, the ITCZ occurs throughout nearly the entire width of the ocean basin, whereas in the Pacific the ITCZ occurs over half the basin width. In the eastern Pacific the ITCZ strength is similar to that in the Atlantic.

The convergence zone found south of the equator in the western Pacific is the South Pacific Convergence Zone (SPCZ); an analogous feature did not occur in the Atlantic Ocean (Figure 2C). An annual mean tropical convergence zone within  $10^\circ$  of the equator was notably absent in the Indian Ocean (Figure 2C and 2D). The CMOFFD-inferred intensity of the southern hemisphere

convergence zone, which was largest in the South Pacific and smallest in the Atlantic Ocean, is consistent with rainfall estimates (Vincent *et al.*, 199)).

#### 4. ITCZ LATITUDE ALONG 28°W

The ITCZ is associated with high sea surface temperature, intense atmospheric convection, a persistent nearly-zonal line of cloud clusters which rapidly appear and disappear, and increased rainfall over an approximate 2°-latitude band. Citeau (1993) defines the ITCZ latitude at 28°W to be the latitude of maximum cloud amount, and determines the location from hourly infrared images recorded by METEOSAT; seven-day average positions were obtained from Dr. Jean Citeau (personal communication, 1993). The 28°W longitude is chosen because it is in the middle of the Atlantic where the influence of the continents upon the diurnal fluctuation of cloud amount is reduced compared to sites close to land. Two methods were used to compute the ITCZ latitude along 28°W with CMODID data. In the 5°S - 10°N band, the latitude where  $v = 0$  defines the position of the confluence zone of the northeast and southeast trade winds. The confluence-zone latitude where  $v = 0$  is easily defined because to the north (south) the winds are westward (eastward) (Figure 3A). In the second scheme, the latitude associated with maximum convergence is determined by visual inspection (Figure 3B), but it is not as easily defined as the confluence zone. Excellent agreement was found between monthly mean ITCZ latitudes computed with CMODID and METEOSAT data (Figure 4). The bias and rms difference between monthly mean METEOSAT-derived latitudes and the CMODID  $v = 0$  latitudes were 0.3° and 2.0°, respectively; the correlation coefficient was 0.94. The METEOSAT and CMODID agreement was poor during July, August and September, which is the time of the year of maximum development of synoptic-scale wave disturbances in the ITCZ (Reed *et al.*, 1988). Two reasons for the discrepancy are suggested. Unlike the 1-h METEOSAT data, the CMODID data were recorded at intervals of 3 days or longer, which would create a substantial amount of aliasing of the 3- to 5-day period African easterly waves. Additionally, in the Atlantic the convergence at the surface is confined to a

shallow layer below 850 mb and clouds occur at several levels which are not stacked vertically (Thompson *et al.*, 1979).

The monthly mean latitudinal positions of the ITCZ revealed the expected annual cycle. The southernmost position was reached in March and the northernmost position occurred in July - September. That the annual march of the ITCZ lags that of the sun by two months is consistent with climatology (Rich], 1979).

## 5. PACIFIC NECC

The NECC flows eastward against the prevailing westward trade wind (hence, the name "countercurrent") in the approximate latitude band 5- 10°N. It occurs south of the westward-flowing North Equatorial Current and north of the westward-flowing South Equatorial Current. Along 158 to 150°W, the center of the 75-m thick thermocline slopes upwards from 140 m at 4°N to 75 m at 9°N, the surface dynamic height anomaly relative to 1000 db is 25 dyn cm higher at 4°N than at 9°N, and the eastward geostrophic surface current is about 0.3 m S<sup>-1</sup> (Wyrki and Kilonsky, 1984). The NECC thickness is less than 200 m.

A tenet of faith among oceanographers that latitudinally varying upper-ocean vertical motion strongly influences the NECC will be examined. Vertical motion in the ocean for time scales longer than several days is very small (Stommel, 1964), and the difficult measurements are scarce, sporadic and intermittent. The upper-ocean vertical velocity will be calculated with CMOFFD data, and a search for a correlative relationship between vertical velocity and NECC transport will be described.

The horizontal divergence of the Ekman wind drift is (Stommel, 1965)

$$(\partial M_{xc}/\partial x + \partial M_{yc}/\partial y) = (1/f) (\text{curl}_z \tau - \beta M_{yc}), \quad (4)$$

where  $M_{xc}$  and  $M_{yc}$  are the east-west and north-south components of the Ekman mass transport per unit width, respectively,  $f$  is the Coriolis parameter that is equal to  $2\Omega \sin \vartheta$  and  $\vartheta$  is the latitude,  $\text{curl}_z \tau$  is the vertical component of the wind-stress curl, and  $\beta$  is the rate of change of the Coriolis

parameter with latitude and is equal to  $2\Omega\cos\delta/R$  with  $R$  equal to the radius of the earth. Assuming the monthly mean vertical velocity at the sea surface is zero (i. e., the rigid-lid approximation), the horizontal divergence of the Ekman wind drift is equal to  $\rho_w w_e$ , where  $\rho_w$  is sea-water density ( $1025 \text{ kg m}^{-3}$ ) and  $WC$  is the vertical velocity at the bottom of the Ekman layer. The assumption of the rigid lid for the sea surface is reasonable because the monthly mean vertical velocity at the sea surface is about 1% of  $WC$ . Substitution of  $M_{yc} = -(\tau_x/f)$  (Stommel, 1965) yields a formulation of the Ekman vertical velocity,

$$WC = (1/\rho_w f)(\text{curl}_z \tau + \beta \tau_x/f). \quad (5)$$

Reasonable estimates of  $WC$  were computed poleward of about  $3^\circ\text{N}$ . Time (monthly mean, April 1992 - July 1993) - longitude (1°-longitude x 1°-latitude mean,  $140^\circ\text{E} - 80^\circ\text{W}$ ) sections (Jovmüller diagram) of monthly mean  $w_e$  were inspected (not shown) at 10 latitudes between  $4^\circ\text{N}$  and  $12^\circ\text{N}$ . Best results were obtained at  $5^\circ\text{N}$  and  $10^\circ\text{N}$ . From approximately  $180^\circ$  to  $100^\circ\text{W}$  the Ekman vertical velocity at  $5^\circ\text{N}$  ( $10^\circ\text{N}$ ) was directed downward (upward) from July to December 1992, and nearly vice versa from January to June 1993 (Figure 5). The simultaneous occurrences of downward motion at  $5^\circ\text{N}$  and upward motion at  $10^\circ\text{N}$  would produce a larger north-south slope of the thermocline and a more intense NECC compared to the opposite situation of upward motion at  $5^\circ\text{N}$  and downward motion at  $10^\circ\text{N}$ . The annual cycle patterns of the CMODFD-inferred  $WC$  and the transport of the NECC arc consistent. The climatological-mean monthly NECC surface current described from ship-drift measurements is weak in April and strong in October (Meehl, 1982.). Similarly, the NECC transport simulated from an ocean general circulation model (OGCM) is weak in April and strong in October (Lolk, 1992).

The Ekman vertical velocities at  $5^\circ\text{N}$  and  $10^\circ\text{N}$  are examined at six longitudes ( $150^\circ\text{E}$ ,  $180^\circ$ ,  $160^\circ\text{W}$ ,  $140^\circ\text{W}$ ,  $125^\circ\text{W}$ ,  $110^\circ\text{W}$ ) in a search for longitudinal variations of the NECC (Figure 6). The combined directions of the  $5^\circ\text{N}$ - and  $10^\circ\text{N}$ -Ekman vertical velocities are believed to be an indicator of north-south thermocline slope and, consequently, of NECC transport. Features of the Ekman vertical motion that are consistent with climatological-mean monthly wind-forced OGCM results (Lolk, 1992) include (i) the longitudinal variation of the annual cycle amplitude, which was

largest at 160°W and 140°W in the central Pacific and weakest at 150°E and 125°W, (ii) the phase of the annual cycle with maximum NECC transport in October and minimum in April, and (iii) the semi-annual variation at 110°W.

## 6. SUMMARY

We employed a nineteen-month FRS-1 scatterometer wind vector data set, which is the longest such data since the 3-month Seasat measurements in 1978. Intercomparison tests with moored-buoy wind observations revealed that CMODFD wind vectors are adequate for monthly mean small horizontal-scale oceanographic and meteorological applications. The CMODFD-inferred position of the ITCZ along 28°W was deemed satisfactory. The 60°S - 60°N CMODFD-derived horizontal divergence (Figure 7) reveals divergence over the Pacific cold tongue, the ITCZ in the Atlantic and Pacific, the SPCZ and the South Indian Convergence Zone, in addition to other features. The relatively wide north-south extent of the ITCZ is an artifact of the annual migration. The annual cycle of wind divergence will be reported elsewhere. The CMODFD data were employed in a study of the time- and space-varying NECC, and produced results consistent with climatology. The NECC transports coincident with FRS-1 data will be reported elsewhere.

## 7. ACKNOWLEDGEMENTS

The TOGA TAO data were acquired electronically from the Pacific Marine Environmental Laboratory, and we are grateful to Dr. S. P. Hayes (deceased) for establishing electronic access to the TAO database. The NDBC data were obtained from the NOAA National Oceanographic Data Center. We are indebted to Dr. J. Citeau, L'Institut Français de Recherche Scientifique Pour le Développement en Coopération (ORSTOM) for kindly sending his estimates of the METEOSAT-derived ITCZ latitudes immediately upon request, W. Knauss, JPL, kept track of million of numbers and prepared the diagrams and tables, all in his usual outstanding manner. This work

was supported by NASA UPN 578-22-26 (DI 1), NASA Grant NAWG-3062 (M111'), NSCAT and STIKSCAT Projects at Oregon State University via JPL Contracts 959294 and 959351 (M111'), and NSCAT (RSD) and STIKSCAT Projects (DI 1, RSD) at JPL, which are gratefully acknowledged. The research described in this paper was performed, in part, by the Jet Propulsion Laboratory, California Institute of Technology, under contract with the National Aeronautics and Space Administration.

## 8. REFERENCES

- Citeau (1993) Position of the Intertropical Convergence Zone along 28°W from January to May 1993. *Veille Climatique Satellitaire*, No. 44,5-6.
- ESA (1992) ERS-1 System. ESA SP- 1146, European Space Agency, Paris, 87 pp.
- Esbensen, S. K., D.B. Chelton, D. Vickers and J. Sun (1993) An analysis of errors in SSM/I evaporation estimates over the global ocean. *Journal of Geophysical Research*, in press.
- Freilich, M. H. and R. S. Dunbar (1993) A preliminary C-band scatterometer model function for the ERS-1 AMI instrument, In: *Proceedings of the First ERS-1 Symposium: Space at the Service of our Environment, Cannes, 4-6 November 1992*, European Space Agency, Paris, 79-84,
- Halpern, D., M. H. Freilich and R. S. Dunbar (1993) Evaluation of two January - June 1993 ERS-1 AMI wind vector data sets. In: *Proceedings of the First ERS-1 Symposium, 3-6 November 1992, Cannes*, European Space Agency, Paris, 135-139.
- Hayes, S. P., L. J. Mangum, J. Picaut and K. Takeuchi (1991) TOGA-TAO: A moored array for real-time measurements in the tropical Pacific Ocean. *Bulletin of the American Meteorological Society*, 72, 339-347.
- Hellerman, S. and M. Rosenstein (1983) Normal monthly wind stress over the world ocean with error estimates. *Journal of Physical Oceanography*, 13, 1093-1104.
- Lolk, N. K. (1992) Annual and longitudinal variations of the Pacific North Equatorial Countercurrent. JPL Publication 92-8, Jet Propulsion Laboratory, 207 pp.
- Mechl, G. A. (1982) Characteristics of surface current flow inferred from a global ocean current data set. *Journal of Physical Oceanography*, 12, 538-555.
- Meindl, B. A. and G. D. Hamilton (1992) Programs of the National Data Buoy Center. *Bulletin of the American Meteorological Society*, 73, 985-993.
- Press, W. H., B. P. Flannery, S. A. Teukolsky and W. T. Vetterling (1986) *Numerical Recipes: The Art of Scientific Computing*. Cambridge University Press, 818 pp.

- Reed, R. J., E. Klinker and A. Jollingsworth (1988) 'The structure and characteristics of African easterly wave disturbances as determined from the ECMWF operational analysis/forecast system, *Meteorology and Atmospheric Physics*, 38, 22.-33.
- Riehl, H. (1979) *Climate and Weather in the Tropics*. Academic Press, 611 pp.
- Stommel, H. M. (1964) Summary charts of the mean dynamic topography and current field at the surface of the ocean, and related functions of the mean wind stress. In: *Studies on Oceanography*, K. Yoshida, editor, University of Tokyo Press, 53-58.
- Stommel, H. M. (1965) *The Gulf Stream*. University of California Press, 248 pp.
- Thompson, R. M., S. W. Payne, E. E. Reeker and R. J. Reed (1979) Structure and properties of synoptic-scale wave disturbances in the intertropical Convergence Zone in the eastern Atlantic. *Journal of the Atmospheric Sciences*, 36, 53-72.
- Trenberth, K. E., W. G. Large and J. G. Olson (1990) The mean annual cycle in global ocean wind stress. *Journal of Physical Oceanography*, 20, 1742-1760.
- Vincent, D. G., K. H. North, R. A. Velasco and P. G. Ramsey (1991) Precipitation rates in the tropics based on the Q<sub>1</sub>-budget method: 1 June 1984-31 May 1987. *Journal of Climate*, 4, 1070-1086.
- Wilkerson, J. C. and M. D. Earle (1990) A study of differences between environmental reports by ships in the voluntary observing program and measurements from NOAA buoys. *Journal of Geophysical Research*, 95, 3373-3385.
- Wyrtki, K. and G. Meyers (1975) The trade wind field over the Pacific Ocean: Part 1. The mean field and the annual variation. Technical Report IIG-75-1, Hawaii Institute of Geophysics, University of Hawaii, 26 pp + 25 figures.

Table 1. Statistics of monthly mean CMODFD-buoy matchups during January - December 1992. Each correlation coefficient,  $r$ , was statistically significant at 95% level.  $N$ = number of matchups; RMS Diff = root-mean-square difference ( $\text{m s}^{-1}$ ) between the matchups; wind speed bias ( $\text{m s}^{-1}$ ) = CMODFD wind speed ( $\text{m s}^{-1}$ ) - buoy wind speed ( $\text{m s}^{-1}$ ).

Buoy Type	N	Variable	$r$	RMS Diff	Bias
NDBC + TAO	142	$u$	0.94	1.29	0.69
NDBC + TAO	142	$v$	0.84	1.23	0.34
NDBC	50	$u$	0.98	0.98	0.14
NDBC	50	$v$	0.91	0.80	-0.01
TAO	92	$u$	0.84	1.43	0.99
TAO	92	$V$	0.82	1.40	0.53

## List of Figures

Figure 1. Locations of moored NDBC buoys. Buoys A, B and C were NDBC Buoys 51004, 51003 and 51001, respectively.

Figure 2. (A) Average July 1992- June 1993 mean CMODFD zonal wind component ( $\text{m s}^{-1}$ ). Dashed contours represent westward wind direction, Contour interval is  $1 \text{ m s}^{-1}$ . (B) North-south profiles of longitudinal-average  $u$  component in each ocean basin: thick solid line, Pacific Ocean; thin solid line, Atlantic Ocean; dotted line, Indian Ocean. (C) Average January - December 1992 mean CMODFD meridional wind component ( $\text{m s}^{-1}$ ). Dashed contours represent southward wind direction. Contour interval is  $1 \text{ m s}^{-1}$ . (D) North-south profiles of zonal-average  $v$  component in each ocean: thick solid line, Pacific; thin solid line, Atlantic; dotted line, Indian.

Figure 3. Monthly mean profiles of the (A) meridional wind component (positive is northward) and (B) horizontal divergence at  $28^\circ\text{W}$  for three months: April, May and June 1993.

Figure 4. Monthly mean estimates positions of the ITCZ along  $28^\circ\text{W}$  determined by three methods: latitude of the maximum cloud amount from 1-week averaged estimates determined from METEOSAT images (solid dot) and the latitudinal range of the weekly estimates is shown with a vertical line; latitude where CMODFD  $v = 0$  (open circle); latitude of maximum convergence (open triangle).

Figure 5. Hovmüller diagrams of Ekman monthly mean Ekman vertical velocity along (A)  $10^\circ\text{N}$  and (B)  $5^\circ\text{N}$ . The downwelling motion is shaded. The right-side of (A) and (B) displays the monthly mean zonal average of the Ekman vertical velocity.

Figure 6. Monthly mean Ekman vertical velocities at  $5^\circ\text{N}$  (dotted line) and  $10^\circ\text{N}$  (solid line) at six

longitudes (150°E, 180°, 160°W, 140°W, 125°W and 110°W).

Figure 7. Annual (July 1992 - June 1993) mean distribution of 10 x 10 averaged horizontal wind divergence ( $10^{-5} \text{ s}^{-1}$ ). The contour interval is  $1 \times 10^{-5} \text{ s}^{-1}$ , and the zero-contour line is not shown.

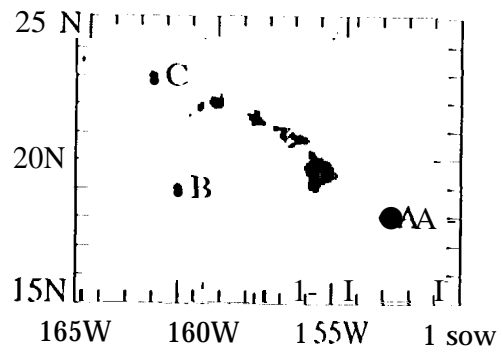


Figure 1

July 1992- June 1993

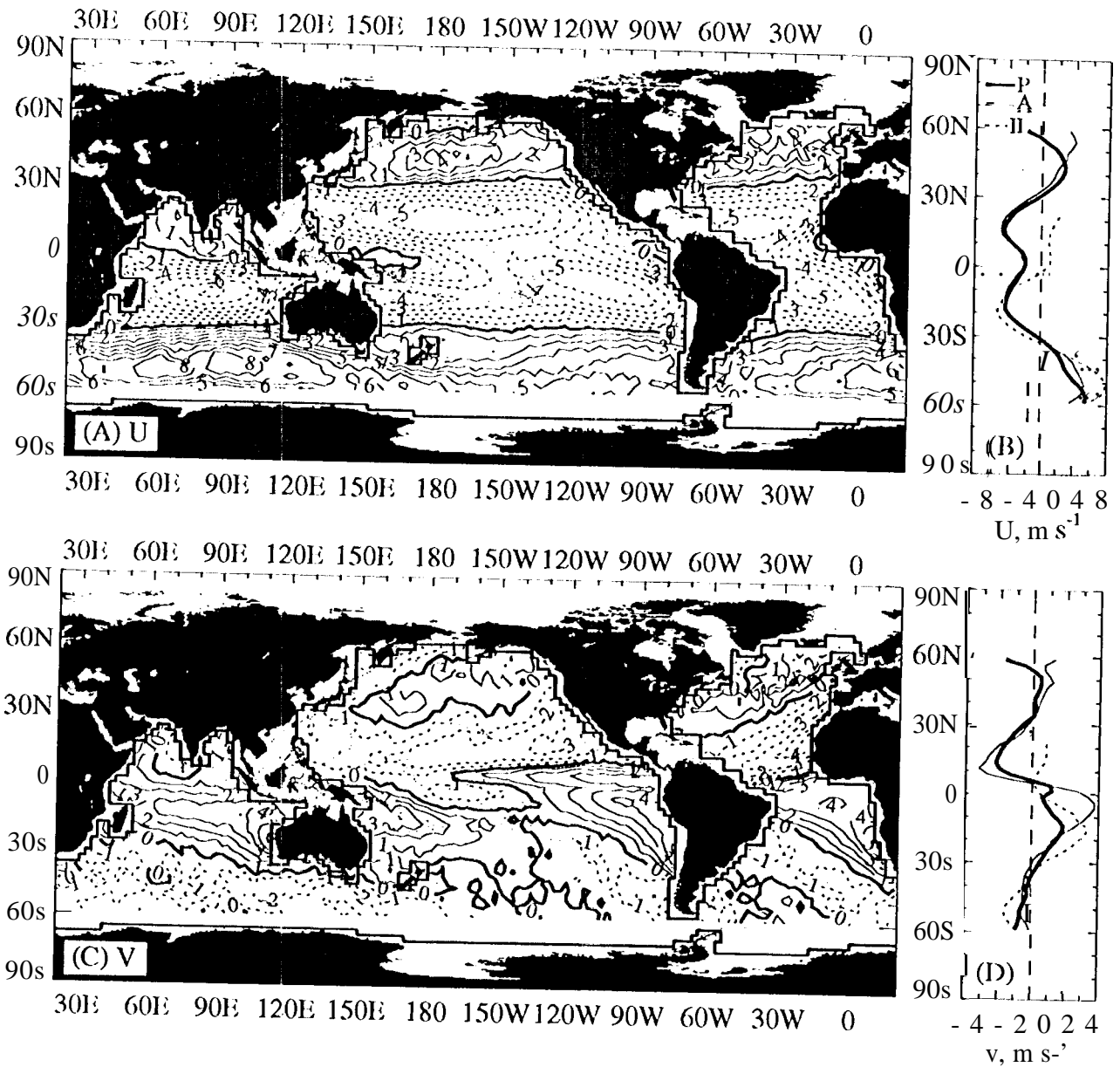


Figure 2

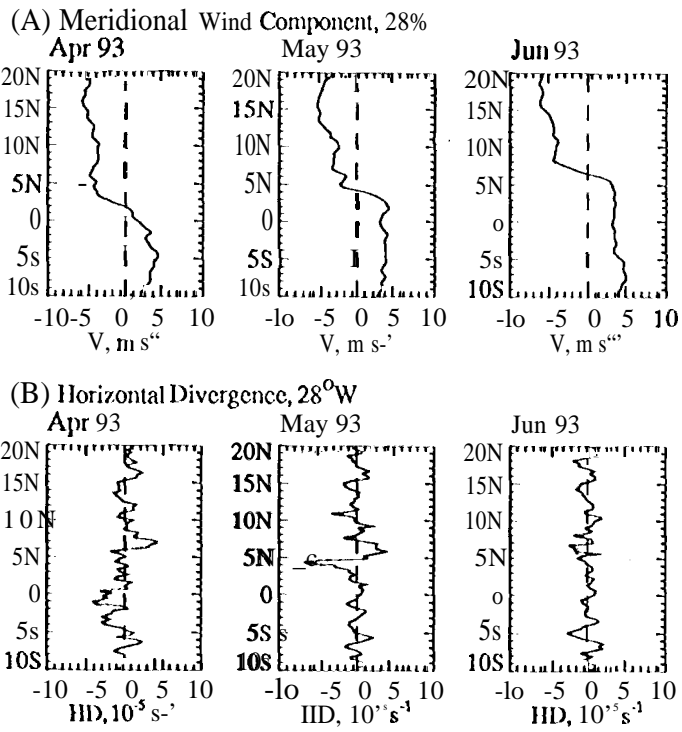


Figure 3

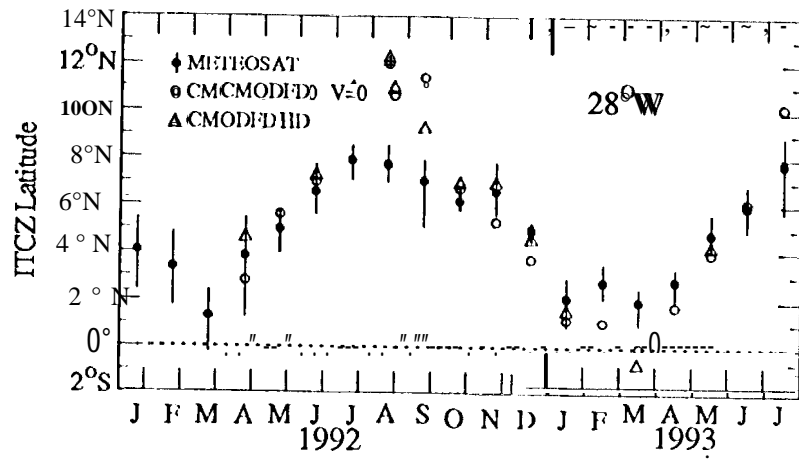


Figure 4

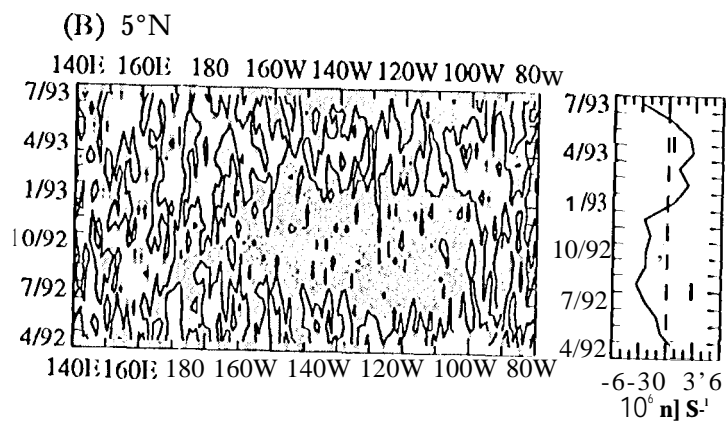
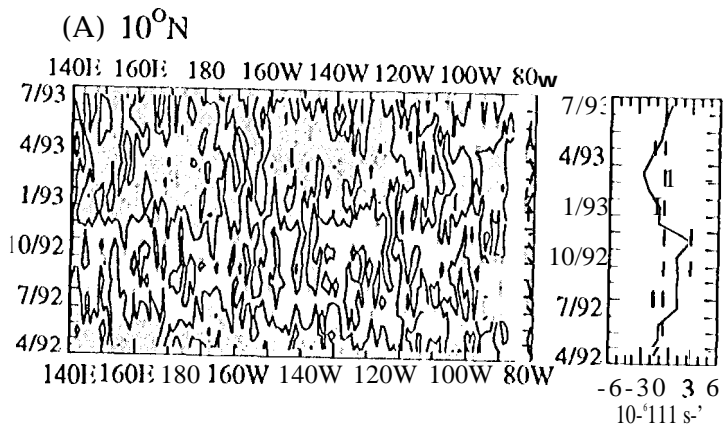
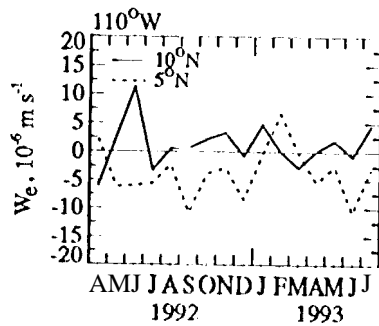
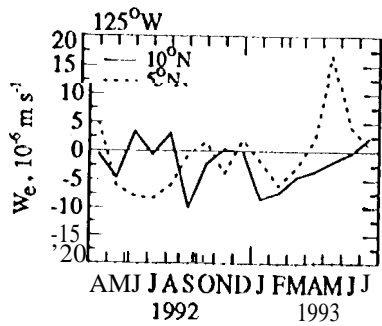
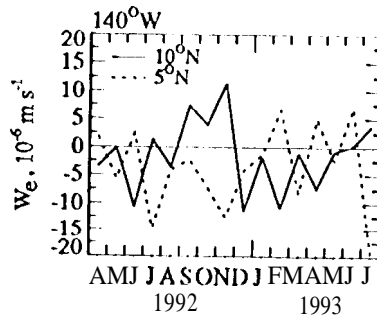
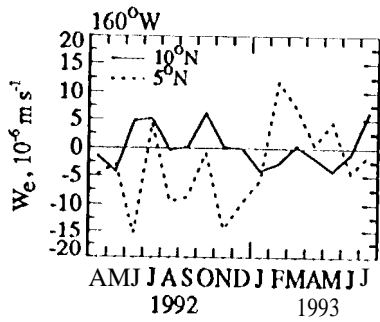
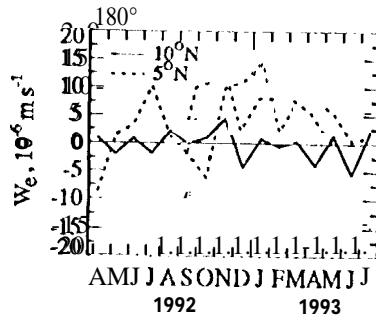
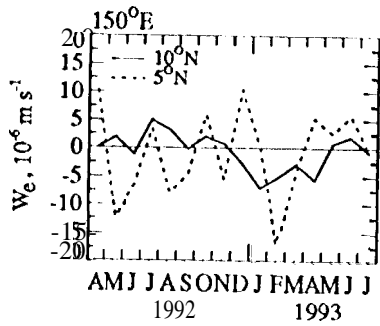


Figure 5



Horizontal Divergence, July 1992 - June 1993

$CI = 1 \times 10^{-5} \text{ s}^{-1}$

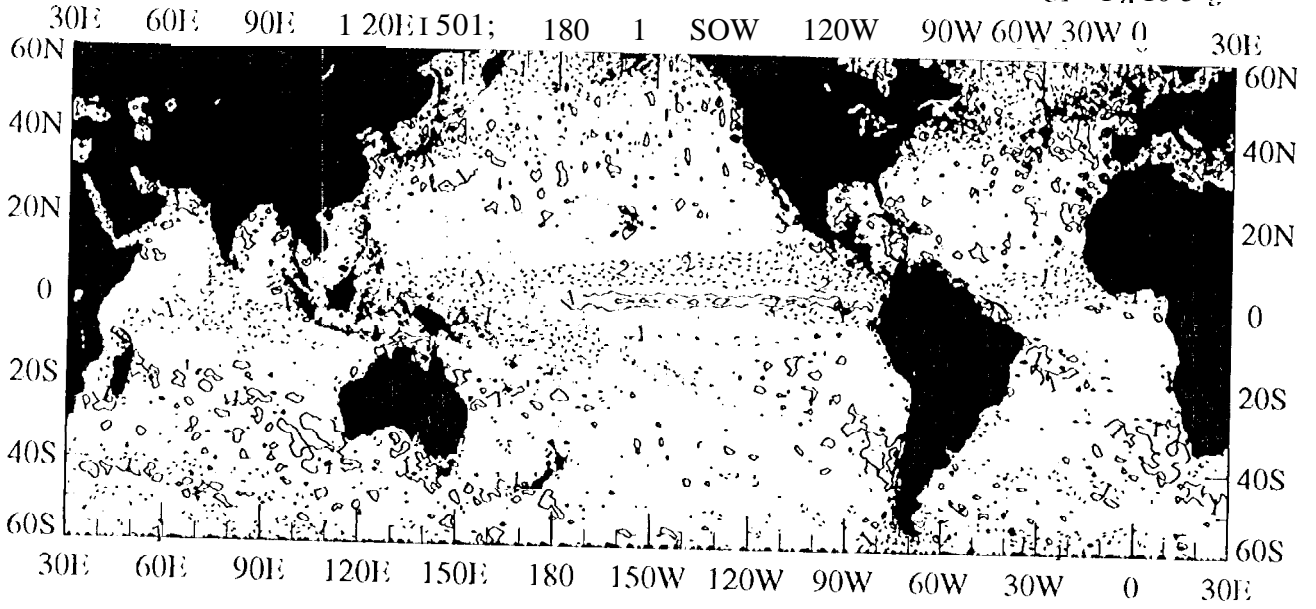


Figure 7